

Convolutional neural networks for long-time dissipative quantum dynamics

Luis E. Herrera Rodríguez^{1,2,3} and Alexei A. Kananenka³

¹*Departamento de Física, Universidad Nacional de Colombia, Carrera 30 No. 45-03, Bogotá D.C., Colombia*

²*Escuela de Ciencias Básicas, Tecnología e Ingeniería,*

Universidad Nacional Abierta y a Distancia, Facatativá, Colombia

³*Department of Physics and Astronomy, University of Delaware, Newark, DE 19711, USA*

(Dated: February 6, 2022)

Exact numerical simulations of dynamics of open quantum systems often require immense computational resources. We demonstrate that a deep artificial neural network comprised of convolutional layers is a powerful tool for predicting long-time dynamics of an open quantum system provided the preceding short-time dynamics of the system is known. The neural network model developed in this work simulates long-time dynamics efficiently and very accurately across different dynamical regimes from weakly damped coherent motion to incoherent relaxation. The model was trained on a data set relevant to photosynthetic excitation energy transfer and can be deployed to study long-lasting quantum coherence phenomena observed in light-harvesting complexes. Furthermore, our model performs well for the initial conditions different than those used in the training. Our approach considerably reduces the required computational resources for long-time simulations and holds promise for becoming a valuable tool in the study of open quantum systems.

INTRODUCTION

Quantum systems encountered in the real world are never completely isolated from their environment. It is the interaction between an open quantum system and its environment that alters the otherwise unitary dynamics of the system and causes energy dissipation and the destruction of phase coherence [1–3]. Understanding the temporal evolution of open quantum systems is a key problem of a broad interest in chemical physics, quantum optics, quantum biology, ultrafast spectroscopy, quantum computing, and quantum information technology [4–9].

Dynamics of an open system, induced by the Hamiltonian evolution of a total system, is referred to as reduced (system) dynamics and is described by the reduced density operator. Many numerically exact methods have been developed to simulate reduced dynamics [8] including the hierarchy of equations of motion (HEOM) technique [10–12], multi-configurational time-dependent Hartree (MCTDH) [13], stochastic Liouville–von Neumann equation [14], time evolving density matrix using orthogonal polynomials algorithm (TEDOPA) [15], diagrammatic quantum Monte Carlo [16–18], path-integral Monte Carlo [19], and the quasi-adiabatic propagator path-integral (QUAPI) approach [20–23]. Unfortunately, many of these methods require computational resources that scale exponentially with the number of simulated time steps and the size of the system rendering such methods not efficient or, even completely impractical, to study long-time quantum dynamical phenomena.

One example of such phenomena is furnished by nature. Photosynthesis is the natural process that provides the energy source for nearly all life on Earth. Photosynthetic conversion of energy starts with the absorption of a photon of sunlight by a light-harvesting pigment and is followed by the excitation energy transfer (EET) to

the reaction center. Recent experiments showed that quantum coherence between electronic states of light-harvesting complexes can persist for several hundreds of femtoseconds even at physiological temperature [24–29]. The physical mechanisms underlying the long-lasting quantum coherence and the role of protein environment in EET are still subjects of active investigations.

Information about the underlying dynamical correlations in open quantum systems is encoded at the initial stages of their evolution. Therefore, it is possible to obtain long-time dynamics of open quantum systems from the knowledge of their short-time evolution bypassing the need for expensive direct long-time simulations. For example, the Nakajima–Zwanzig generalized quantum master equation (GQME) [30, 31] furnishes a general and formally exact prescription for achieving this goal provided the memory kernel is known [32, 33]. Unfortunately, it is difficult to directly calculate the memory kernel exactly for arbitrary systems and solve the GQME. The latter issue is resolved in the transfer tensor method (TTM) [34–37]. The TTM, however, requires a set of dynamical maps to be supplied by an external numerical technique. For a N -level system an input set of dynamical maps generated for the N^2 linearly independent initial conditions of the system is required. Since this input must be provided by some, preferably exact, method the computational cost of generating such an input grows steeply with the system size.

In the last decade, the field of deep learning has enjoyed a dramatic expansion owing to multiple successful applications in the recognition of complex patterns [38]. Learning temporal and spatio-temporal information has been an active area of research recently due to a myriad of potential applications including detection and characterization of behavior from video sequences [39–59], natural language processing [60, 61], and weather forecast-

ing [62, 63]. Recurrent neural network (RNN) is a class of artificial neural networks (ANN) developed specifically to analyze temporal data. RNNs take into account the sequential context using recurrent connections in the hidden layers. RNNs based on Long Short-Term Memory (LSTM) [60] cells outperform other RNNs and found numerous applications [50, 58, 64].

Three-dimensional (3D) convolutional neural networks (CNN) [53] are based on a straightforward extension of the established 2D CNNs [65, 66] to the 3D spatio-temporal domain. 3D CNNs have also been successful in analyzing spatio-temporal data [53] and are known to outperform LSTMs in certain tasks [55]. LSTMs process elements one at a time with a form of memory and thus perceived to be more suitable for extracting long-range temporal dependencies as opposed to convolutions that operate on local neighborhoods. On the other hand LSTMs are more difficult to train than CNNs [59].

Despite widespread popularity in the domain of the physical sciences [67] machine learning applications to open quantum systems have only recently begun to emerge [68]. Restricted Boltzmann machine representations of the density matrix were used to determine steady states [69–72] and Markovian dynamics [71] of open quantum systems. Deep RNNs were used to simulate the dynamics of the spin-boson and Landau–Zener models [73, 74], as well as to learn Lindblad operators of Master equations and predict the future time evolution of a system [75].

Given the high computational cost of numerically exact simulations and the ability of machine learning techniques to learn complex physical phenomena it is highly desirable to develop a machine learning approach that can accurately predict long-time dynamics of open quantum systems and, at least partially, eliminate the need for expensive direct calculations. The purpose of this article is to introduce such a method. The physics of dissipative open quantum systems is incredibly rich [1–3] naturally rendering such learning problem very difficult. We illustrate that a properly trained ANN can very accurately predict long-time dynamics of open quantum systems. In contrast to existing methods [73, 75] our approach employs a simpler and easier to train convolutional ANN and, most importantly, the single ANN developed in this work accurately predicts non-Markovian reduced system dynamics in a broad range of dynamical regimes from weakly damped coherent motion to the incoherent decay.

THEORETICAL BACKGROUND

We consider the common system-bath model with the Hamiltonian given by

$$\hat{H} = \hat{H}_s + \hat{H}_{sb} + \hat{H}_b, \quad (1)$$

where \hat{H}_s is the system Hamiltonian, \hat{H}_b describes the thermodynamic reservoir or heat bath, and \hat{H}_{sb} is the coupling between the system and the bath.

The system Hamiltonian takes the form

$$\hat{H}_s = \sum_{n=1}^N \epsilon_n |n\rangle\langle n| + \sum_{k \neq n=1}^N J_{nk} |k\rangle\langle n|, \quad (2)$$

where the energy of a state n in the absence of the bath is denoted by ϵ_n and J_{nk} is the coupling between the n th and the k th states.

The bath is responsible for the system’s energy fluctuation and dissipation. It is modeled by a set of quantum harmonic oscillators

$$\hat{H}_b = \sum_{j=1}^{N_b} \left(\frac{\hat{p}_j^2}{2m_j} + \frac{1}{2} m_j \omega_j^2 \hat{x}_j^2 \right), \quad (3)$$

where the momentum, position, mass, and frequency of the j th harmonic oscillator are given by \hat{p}_j , \hat{x}_j , m_j , and ω_j , respectively. It should be noted that the harmonic representation of the bath does not imply that the microscopic potentials of the environment are assumed to be harmonic. Rather the rationale behind this choice of the representation of the bath is that the reservoir with many macroscopic degrees of freedom carry Gaussian fluctuation properties.

The system-bath coupling is taken to be linear in bath coordinates

$$\hat{H}_{sb} = \sum_{n=1}^N \sum_{j=1}^{N_b} c_j \hat{x}_j |n\rangle\langle n|. \quad (4)$$

The coupling constants c_j can be characterized by a single function of frequency known as the spectral density

$$C(\omega) = \frac{\pi}{2} \sum_{j=1}^{N_b} \frac{c_j^2}{m_j \omega_j} \delta(\omega - \omega_j). \quad (5)$$

Time-evolution of an open quantum system is described by its reduced density operator $\hat{\rho}_s$ which is defined as the partial trace of the total density operator $\hat{\rho}$ over the bath degrees of freedom

$$\hat{\rho}_s(t) = \text{Tr}_b [\hat{\rho}(t)]. \quad (6)$$

The reduced density operator evolves in time according to

$$\hat{\rho}_s^I(t) = \hat{U}^I(t) \hat{\rho}_s^I(0), \quad (7)$$

where the superscript “I” indicates the interaction picture with respect to $\hat{H}_s + \hat{H}_b$ in the Liouville space which is defined for any Schrödinger picture operator \hat{O}_S as $\hat{O}_I(t) \equiv e^{i\mathcal{L}_s t} \hat{O}_S$ with \mathcal{L}_s being the system Liouvillian. The reduced propagator $\hat{U}^I(t)$ is given by

$$\hat{U}^I(t) \equiv \left\langle \mathcal{T}_+ \exp \left[-\frac{i}{\hbar} \int_0^t d\tau \mathcal{L}_{sb}^I(\tau) \right] \right\rangle, \quad (8)$$

where $\langle \dots \rangle = \text{Tr}_b [\dots e^{-\beta \hat{H}_b}] / Z$ is a thermal quantum-mechanical average over bath modes, $\beta \equiv (k_B T)^{-1}$ is the inverse temperature, $Z \equiv \text{Tr}_b [e^{-\beta \hat{H}_b}]$ is the partition function, and \mathcal{T}_+ orders the $\mathcal{L}_{sb}^I(t)$'s in increasing time from right to left.

In what follows we show that given the complete knowledge of the short-time evolution of the reduced density matrix (RDM) at the discretized times $\{\rho_{ij}^s(t_k), \rho_{ij}^s(t_{k+1}), \dots, \rho_{ij}^s(t_m), \forall i, j \in [1, N]\}$, where $\rho_{ij}^s(t_k) = \langle i | \hat{\rho}_s(t_k) | j \rangle$, $t_k = k\Delta t$ and Δt is the time step, a trained ANN is capable of propagating the RDM to arbitrary long times $\rho_{ij}^s(t_m) \rightarrow \rho_{ij}^s(t_{m+1}), \dots, \rho_{ij}^s(\infty)$. Thus our approach completely avoids a computationally expensive numerically exact propagation of the reduced density operator beyond some finite time $t_{\text{mem}} = t_{m-k}$ which will be referred to as memory or learning time. The finite memory time is not an assumption but, rather, a direct consequence of the finite time span of bath correlations in realistic systems.

METHODS

Model system

Even though the approach described in this work is general, we present it on the example of a two-level system ($N = 2$, $|n\rangle \in \{|0\rangle, |1\rangle\}$) coupled to harmonic bath. The spectral density is taken to be the Drude-Lorentz density [9] (an Ohmic distribution with a Lorentzian cut-off)

$$C(\omega) = 2\lambda \frac{\omega\omega_c}{\omega^2 + \omega_c^2}, \quad (9)$$

where λ is the reorganization energy which represents the magnitude of fluctuations and dissipation, and ω_c is the cut-off frequency which characterizes how quickly the bath relaxes toward equilibrium.

The total system under study is, thus, fully determined by the five independent energy scales: the energetic bias $\Delta = \epsilon_1 - \epsilon_0$, the coupling strength J , the reorganization energy λ , the cut-off frequency ω_c , and thermal energy $k_B T$ of the bath. Therefore, in order to create a data set suitable for machine learning framework aimed at predicting quantum dynamics in all physically realizable regimes, four out of five parameters above have to be extensively sampled. While nowadays this task most certainly does not present a major challenge, in this work we generated only a subset of the total required data set by fixing two parameters: the coupling strength J and the cut-off frequency ω_c .

For concreteness we illustrate our approach on the example of photosynthetic EET and consider a two-molecule system or dimer. The system Hamiltonian,

Eq. 2, describes an electronic system within a single-excitation manifold which for a dimer comprises of singly-excited electronic states of each molecule. Thus, in Eqs. 2 and 4 $|n\rangle$ represents the state where only one of the two molecules is in its excited electronic state while the other molecule is in its ground electronic state. The ground and excited states of the total system are denoted as $|0\rangle$ and $|1\rangle$ respectively. The single-excitation manifold approximation is often well-justified. For example, in certain photosynthetic organisms, such as purple bacteria, the rate of photon capture is low enough to guarantee that at most one excitation is present on the photosynthetic membrane [76].

Following previous work (e.g., Refs. [11, 29, 77, 78]) we choose $J = 100 \text{ cm}^{-1}$ and set the cut-off frequency ω_c to 53 cm^{-1} . These are the typical parameters of photosynthetic EET. We note that, according to Ref. [79], specific values of J and ω_c chosen here correspond to a moderately non-Markovian regime.

Data generation and preprocessing

Building a representative data set is an important first step in every machine learning project. The HEOM method implemented in the PHI code [82] is used to solve Eqs. 7 and 8. The hierarchy truncation is set to 20 and 3 Matsubara terms are used. The integration time step is set to 0.1 fs. The convergence of all the results, presented in this article, with respect to these parameters is verified. The data set containing time-evolved RDMs is generated for all combinations of the following parameters: $\Delta \in \{0, 25, 50, 75, 100, 125, 150, 175, 200, 225, 250, 275, 300\} \text{ cm}^{-1}$, $\lambda \in \{2, 10, 20, 30, 40, 50, 60, 70, 80, 90, 100, 120, 130, 150, 200, 250, 300, 350, 400, 450, 500\} \text{ cm}^{-1}$, and $T \in \{25, 50, 75, 100, 125, 150, 175, 200, 225, 250, 275, 300, 325, 350, 375, 400\} \text{ K}$. We note that while the suggested reorganization energies in EET are typically similar to the electronic coupling [80, 81], for the purpose of building a diverse data set, the range of reorganization energies is extended to as low as 2 cm^{-1} and as high as 500 cm^{-1} . The resulting data set is diverse enough to represent weakly damped coherent dynamics ($J/\lambda > 1$), incoherent decay ($J/\lambda < 1$), and the transition between the two regimes.

For each combination of parameters the reduced density operator is propagated starting from the factorized product state $\hat{\rho}(0) = \hat{\rho}_s(0) \otimes \hat{\rho}_b^{eq}$. The electronic system is assumed to start out at the first excited state $\hat{\rho}_s(0) = |1\rangle\langle 1|$, and the bath is at thermal equilibrium $\hat{\rho}_b^{eq} = e^{-\beta \hat{H}_b} / Z$. It should be noted that, in general, this factorized initial state is unphysical due to the neglect of an inherent correlation between the system and the bath. However, in modeling electronic excitation processes such initial state is appropriate because it corre-

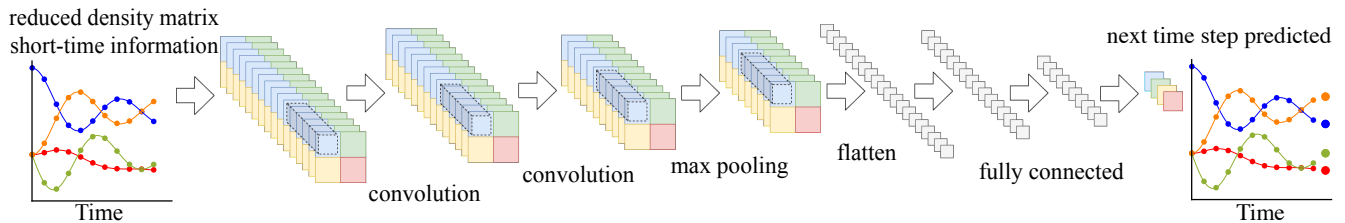


FIG. 1. Long-time quantum dynamics with artificial neural networks. A set of short-time system reduced density matrices at the discretized times serves as an input. It is then processed through the two convolutional layers followed by the max-pooling layer and two fully-connected layers. The result is the reduced density matrix predicted for the time step following the last time step of the input set of reduced density matrices.

sponds to the electronic ground or excited state generated by photoexcitation in accordance to the vertical Frank-Condon transition.

The total propagation time is set to 1.0 ps for all parameter sets even though in some cases the coherent dynamics persists for longer times. It is though still longer than a typical coherence time of several hundreds femtoseconds found in photosynthetic EET [11].

For each set of parameters the generated quantum RDM trajectory is divided into shorter RDM trajectories with the length equal to the memory time. Since the total propagation time is fixed to 1.0 ps, the actual size of the data set used varies depending on the length of the memory time. For example, for the memory time of 0.2 ps the data set is comprised of 21,840 0.2 ps long RDM trajectories. These trajectories are time discretized with the time step of 5 fs. A small set of 150 RDM trajectories is randomly taken from the total data set and is used to produce the results presented in this article. The remaining data set is partitioned into a training set of 80% of the data and a validation set of 10% of the data. Additionally, 10% of the data is held out during the training procedure and is used for testing.

Neural network model and training

The ANN architecture used in this work is based on three-dimensional (3D) convolutional and 3D pooling layers. It is schematically illustrated in Figure 1. 3D convolutional layers are essentially 2D convolutional layers extended such that all filters operate over space and time. Similarly, 3D pooling is a straightforward extension of 2D pooling to the temporal domain. 3D convolutional layers extract short-time correlations, while pooling layers combine information across longer time periods.

The ANN architecture is optimized using the Hyperopt library [86]. The number of 3D convolutional layers is chosen between 1 and 3. The size of a 3D convolutional kernel is represented by a triple (d_t, d_{s1}, d_{s2}) , where d_t is the temporal depth and (d_{s1}, d_{s2}) denotes the spatial size. We set the spatial size to be $d_{s1} = d_{s2} = 1$ for the reasons explained below. The temporal depths of the filters for

each layer are chosen as $d_t = 2^n$ with all integer values of $n \in [4, 8]$ tested. The single 3D maximum pooling layer with the kernel size of $(2,1,1)$ follows 3D convolutional layers. The number of fully-connected layers is chosen between 1 and 3 and the number of neurons in each fully-connected layer is chosen as 2^n with all integer values of $n \in [4, 7]$ tested. Commonly used activation functions including hyperbolic tangent, sigmoid, and the rectified linear activation function (ReLU) [87] are tested. For the output nodes the linear function $f(x) = x$ is used to eliminate any restriction on the range of possible output values. The output layer contains the three real-valued numbers that uniquely define the next time-step RDM: one diagonal element $\rho_{00}^s(t)$, as well as the real and imaginary parts of one off-diagonal element $\text{Re}\{\rho_{01}^s(t)\}$, and $\text{Im}\{\rho_{01}^s(t)\}$. The other diagonal element $\rho_{11}^s(t)$ is also added to the output layer in order to check whether our ANN model can learn some fundamental properties of the density matrix e.g., the unit trace property.

The optimized ANN comprises the two 3D convolutional layers followed by one 3D maximum pooling layer, two fully-connected layers and the output layer. The optimal number of filters in both 3D convolutional layers is 30. The temporal depths of the kernels in the first and second 3D convolutional layers are 16 and 4 time steps, or 80 and 20 fs correspondingly. The two fully-connected layers containing 256 and 64 neurons follow the 3D pooling layer. The ReLU activation function is selected for each of the 3D convolutional and fully-connected layers. The total number of trained parameters in the optimized ANN is 2,816,624.

The 1×1 spatial convolution employed in all 3D convolutional layers means that the correlation between individual elements of the RDM at a given time are not accounted for. It should be noted that in some cases only a limited knowledge of short-time RDMs is available. This partially motivates our choice to separately process different elements of the RDM through the 3D convolutional and pooling layers. Further motivation stems from the observation that increasing d_{s1} and/or d_{s2} to 2 in 3D convolutional and pooling layers does not increase the prediction accuracy.

The backpropagation is used to train the ANN to pre-

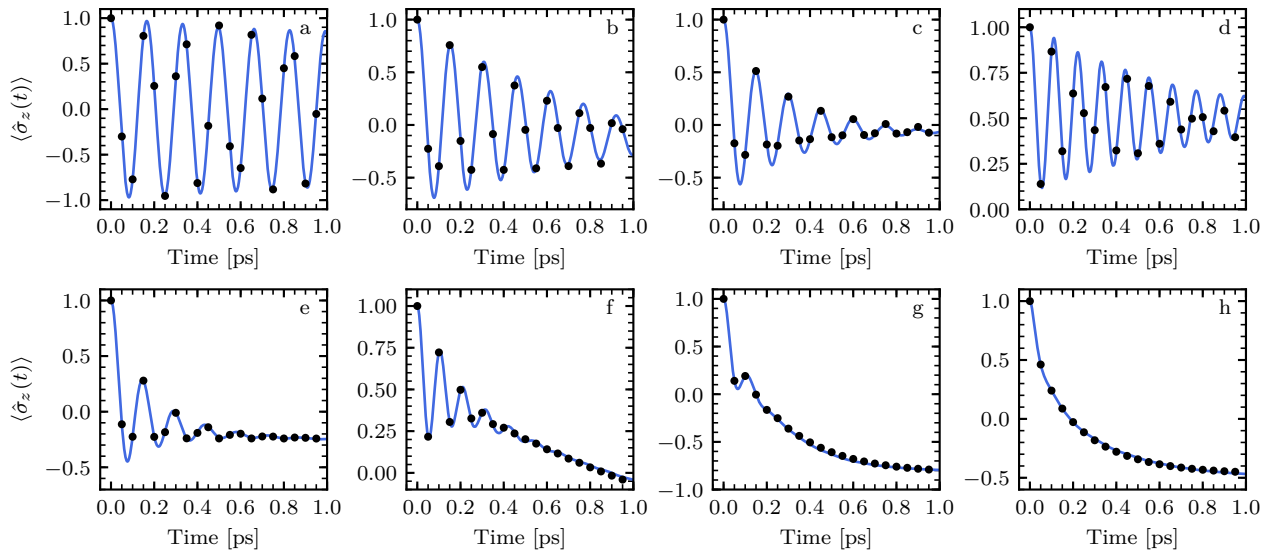


FIG. 2. Expectation value of $\hat{\sigma}_z$ as a function of time predicted by the neural network model developed in this work (blue solid lines) for various sets of parameters compared to the exact results (black circles) obtained with the HEOM method: (a) $\Delta=0$ cm⁻¹, $\lambda=2$ cm⁻¹, $T=125$ K; (b) $\Delta=75$ cm⁻¹, $\lambda=10$ cm⁻¹, $T=100$ K; (c) $\Delta=25$ cm⁻¹, $\lambda=20$ cm⁻¹, $T=275$ K; (d) $\Delta=225$ cm⁻¹, $\lambda=2$ cm⁻¹, $T=175$ K; (e) $\Delta=50.0$ cm⁻¹, $\lambda=70.0$ cm⁻¹, $T=100$ K; (f) $\Delta=250$ cm⁻¹, $\lambda=20$ cm⁻¹, $T=75$ K; (g) $\Delta=225$ cm⁻¹, $\lambda=80$ cm⁻¹, $T=50$ K; (h) $\Delta=175$ cm⁻¹, $\lambda=200$ cm⁻¹, $T=25$ K. Other parameters are $J = 100$ cm⁻¹ and $\omega_c = 53$ cm⁻¹.

dict the RDM for the time step immediately following the chronologically last time step of the input set of RDMs. In the backpropagation the adaptive moment solver [83] is used and the mean squared error function is employed as the loss function. ANN models are trained using the Keras software package [84] with the TensorFlow [85] backend. Further hyperparameter tuning is performed by means of a random-search algorithm [88]. The best results were obtained with the learning rate of $1 \cdot 10^{-7}$ and a batch size of 512.

RESULTS AND DISCUSSION

The ANN introduced above is used to simulate the relaxation dynamics of the dimer coupled to the harmonic bath described in the previous section. We consider the expectation value of the $\hat{\sigma}_z$ Pauli operator $\langle \hat{\sigma}_z(t) \rangle = p_1(t) - p_0(t)$, where $p_{1(0)}(t)$ is the time-dependent population of the corresponding state. The results for the eight sets of parameters representing different regimes ranging from weakly damped coherent oscillations to incoherent relaxation are illustrated in Figure 2. In each case the memory time of 0.2 ps is used and the corresponding set of RDMs is supplied to the ANN as an input. The ANN predicts the RDM at the next time step. Then, a new input is formed by combining the newly predicted RDM with all the RDMs taken within the 0.2 ps time span back starting from the just predicted RDM. This process is repeated until the specified propagation end time is

reached. We emphasize that only the short-time initial dynamical information is required. The rest of the time-evolution is simulated by reconstructing the RDM based on ANN predictions for each time step beyond the initial learning time. Thus, if a single-step prediction error is not sufficiently small then the error will very quickly accumulate resulting in a rapid deterioration of the accuracy. However, as evident from Figure 2 our method reproduces long-time dynamics nearly exactly and irrespective of the dynamical regime. The data shown in Figure 2 represents a small fraction of a test set. The interested reader is referred to Supporting Information Figures S1-S5 where many more results are presented. In addition to $\langle \hat{\sigma}_z(t) \rangle$, Figures S1-S5 also report the ANN predictions for the real and imaginary parts of the off-diagonal elements of the RDM. These results demonstrate that our ANN model can very accurately predict long-time evolution of the entire RDM. Additionally, we note that by virtue of its ability to accurately predict dynamics to arbitrary times, our ANN model also correctly reproduces equilibrium populations.

The accuracy of our method depends on the memory time as can be expected. Supporting Information Figure S6 illustrates that the ANN prediction error decreases monotonically with increasing memory time. We choose a memory time of 0.2 ps in all calculations reported in this article as it provides a compromise between accuracy and computational cost required to generate the input set of RDMs. More rigorously, the learning time can be determined from the decay of the magnitude of transfer

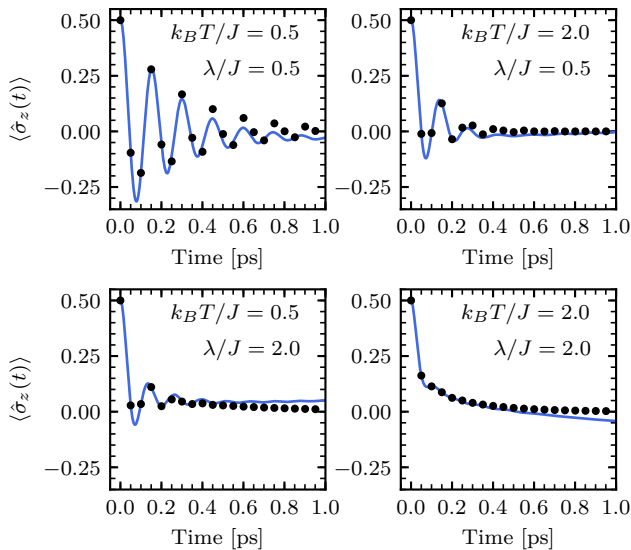


FIG. 3. Expectation value of $\hat{\sigma}_z$ as a function of time predicted by the neural network model developed in this work (blue lines) compared to the exact result (black lines) for the initial system reduced density matrix $\rho_s(0) = (1/4)|0\rangle\langle 0| + (3/4)|1\rangle\langle 1|$, $J=100 \text{ cm}^{-1}$, $\Delta = 0 \text{ cm}^{-1}$, and $\omega_c = 53 \text{ cm}^{-1}$.

tensors, as it is done in the TTM method [34, 37], or a norm of the GQME memory kernel. A pre-defined and identical memory time for all cases studied here is chosen to accommodate the fixed-size input requirement of ANNs. It is highly desirable to provide a further flexibility to our approach by designing a descriptor that can integrate various memory times and be a suitable input to ANN. The work in this direction is underway.

As discussed in Ref. [79], which utilizes the measure of non-Markovianity based on quantum state trace difference [1], for fixed J and ω_c non-Markovianity is maximized for intermediate values of $\lambda \sim 40\text{--}80 \text{ cm}^{-1}$ and site energy differences Δ below $\sim 150 \text{ cm}^{-1}$. Additionally, we note that the typical values of ω_c for photosynthetic EET satisfy the high-temperature assumption $\beta\hbar\omega_c < 1$ [11], which for $\omega_c = 53 \text{ cm}^{-1}$ corresponds to temperature $T > 77 \text{ K}$. All of these conditions are satisfied in Figure 2e, which thus provides a test of our ANN model in a realistic scenario of considerable non-Markovian dynamics. We observed a very good agreement between the ANN predicted long-time dynamics and the exact results in this case as well.

The ability of our ANN model to learn the fundamental properties of the density matrix is tested on the unit trace and positive semidefiniteness properties. We emphasize that these properties are not enforced during the training. Impressively, we found that our ANN model was able to learn both properties essentially precisely. The largest deviation of the trace of the predicted RDMs from unity in a held out data set of 150 samples is only $1\cdot 10^{-5}$ and

not a single predicted RDM is found to have negative diagonal elements.

As a stringent test of our ANN model we assess its ability to generalize to the input data not present in the original data set. To this end we evaluate our ANN model on an input set of short-time RDMs corresponding to the following initial mixed state of the electronic system $\hat{\rho}_s(0) = (1/4)|0\rangle\langle 0| + (3/4)|1\rangle\langle 1|$. The bath is still kept at thermal equilibrium. Figure 3 shows the results obtained for the four cases ranging from small to large reorganization energy and low to high temperature. The electronic system parameters are fixed to be $J = 100 \text{ cm}^{-1}$, $\Delta = 0 \text{ cm}^{-1}$ and the cut-off frequency ω_c is set to 53 cm^{-1} . As anticipated, our ANN model performs slightly worse in the region of small reorganization energy and low temperature which is the most difficult regime of weakly damped coherent oscillatory dynamics. Overall across all the cases studied with the out-of-data set initial condition of the system we notice that the single time-step prediction error slightly increases, compared to the results shown in Figure 2, which results in noticeable deviations of the predicted populations from the exact ones at long times. However, these deviations are still small and do not exceed 3.6%. Thus, we conclude that our ANN model performs reasonably well even for the initial condition of the system different from the initial condition used to generate the original data set. It should be noted that extending our ANN model to regimes of arbitrary electronic coupling and bath correlation time is less straightforward and would require a retraining with a more appropriate data set.

CONCLUSIONS

In summary, we showed that an ANN trained on a set of time-discretized RDMs is capable of predicting the future time-evolution of a given RDM with high accuracy. Only a short-time calculation with numerically accurate method is required and the rest of the dynamics can be efficiently predicted by our ANN model. Thus our approach considerably reduces the required resources for long-time simulations of dissipative open quantum systems. What makes our approach particularly appealing is (i) the relative simplicity of the ANN model employed as opposed to ANNs with internal memory that are more difficult to train and (ii) its ability to accurately predict long-time dynamics of open quantum systems across various dynamical regimes including nonadiabatic and non-Markovian dynamics. A photosynthetic EET was chosen as an example but the same approach can be used to study other phenomena provided the relevant data sets are available. The total data set used in this work is built from 4,368 HEOM calculations. Given the currently available computational resources the generation of similar data sets to study other problems is a trivial task.

Our approach is yet another illustration of the ability of ANNs to model complex physical phenomena at a small fraction of the cost of a full numerically exact calculation.

ACKNOWLEDGEMENTS

This work was supported by the startup funds of the College of Arts and Sciences and the Department of Physics and Astronomy of the University of Delaware. L. E. H. R. would like to acknowledge support by the Beyond Research Program between University of Delaware and Universidad Nacional de Colombia. Calculations were performed with high-performance computing resources provided by the University of Delaware.

-
- [1] H.-P. Breuer and F. Petruccione, *The Theory of Open Quantum Systems* (Oxford University Press, New York, NY, 2002).
- [2] U. Weiss, *Quantum Dissipative Systems* (World Scientific, Singapore, 2012).
- [3] A. J. Leggett, S. Chakravarty, A. T. Dorsey, M. Fisher, A. Garg, and W. Zwerger, Dynamics of the dissipative two-level system, *Rev. Mod. Phys.* **59**, 1 (1987).
- [4] V. May and O. Kühn, *Charge and Energy Transfer Dynamics in Molecular Systems* (Wiley-VCH, Weinheim, Germany, 2011).
- [5] A. Nitzan, *Chemical Dynamics in Condensed Phases: Relaxation, Transfer, and Reactions in Condensed Molecular Systems*, Oxford Graduate Texts (OUP Oxford, 2013).
- [6] L. Valkunas, D. Abramavicius, and M. T., *Molecular Excitation Dynamics and Relaxation: Quantum Theory and Spectroscopy* (Wiley-VCH, Weinheim, Germany, 2013).
- [7] M. A. Nielsen and I. L. Chuang, *Quantum Computation and Quantum Information: 10th Anniversary Edition* (Cambridge University Press, New York, NY, USA, 2011).
- [8] I. d. Vega and D. Alonso, Dynamics of non-Markovian open quantum systems, *Rev. Mod. Phys.* **89**, 0317 (2017).
- [9] S. Mukamel, *Principles of Nonlinear Optical Spectroscopy* (Oxford University Press, New York, NY, USA, 1995).
- [10] Y. Tanimura and R. Kubo, Two-time correlation functions of a system coupled to a heat bath with a Gaussian-Markoffian interaction, *J. Phys. Soc. Jap.* **58**, 1199 (1989).
- [11] A. Ishizaki and G. R. Fleming, Unified treatment of quantum coherent and incoherent hopping dynamics in electronic energy transfer: Reduced hierarchy equation approach, *J. Chem. Phys.* **130**, 234111 (2009).
- [12] Y. Tanimura, Numerically “exact” approach to open quantum dynamics: The hierarchical equations of motion (HEOM), *J. Chem. Phys.* **153**, 020901 (2020).
- [13] H.-D. Meyer, U. Manthe, and L. Cederbaum, The multi-configurational time-dependent Hartree approach, *Chem. Phys. Lett.* **165**, 73 (1990).
- [14] J. T. Stockburger and H. Grabert, Exact c -number representation of non-Markovian quantum dissipation, *Phys. Rev. Lett.* **88**, 170407 (2002).
- [15] J. Prior, A. W. Chin, S. F. Huelga, and M. B. Plenio, Efficient simulation of strong system-environment interactions, *Phys. Rev. Lett.* **105**, 050404 (2010).
- [16] G. Cohen and E. Rabani, Memory effects in nonequilibrium quantum impurity models, *Phys. Rev. B* **84**, 075150 (2011).
- [17] G. Cohen, E. Gull, D. R. Reichman, and A. J. Millis, Taming the dynamical sign problem in real-time evolution of quantum many-body problems, *Phys. Rev. Lett.* **115**, 266802 (2015).
- [18] H.-T. Chen, G. Cohen, and D. R. Reichman, Inchworm Monte Carlo for exact non-adiabatic dynamics. I. Theory and algorithms, *J. Chem. Phys.* **146**, 054105 (2017).
- [19] D. Kast and J. Ankerhold, Persistence of coherent quantum dynamics at strong dissipation, *Phys. Rev. Lett.* **110**, 010402 (2013).
- [20] D. E. Makarov and N. Makri, Path integrals for dissipative systems by tensor multiplication. Condensed phase quantum dynamics for arbitrarily long time, *Chem. Phys. Lett.* **221**, 482 (1994).
- [21] N. Makri, Improved Feynman propagators on a grid and non-adiabatic corrections within the path integral framework, *Chem. Phys. Lett.* **193**, 435 (1992).
- [22] N. Makri, Numerical path integral techniques for long time dynamics of quantum dissipative systems, *J. Math. Phys.* **36**, 2430 (1995).
- [23] N. Makri, Quantum dissipative dynamics: A numerically exact methodology, *J. Phys. Chem. A* **102**, 4414 (1998).
- [24] H. Lee, Y.-C. Cheng, and G. R. Fleming, Coherence dynamics in photosynthesis: Protein protection of excitonic coherence, *Science* **316**, 1462 (2007).
- [25] G. S. Engel, T. R. Calhoun, E. L. Read, T.-K. Ahn, T. Mančal, Y.-C. Cheng, R. E. Blankenship, and G. R. Fleming, Evidence for wavelike energy transfer through quantum coherence in photosynthetic systems, *Nature* **446**, 782 (2007).
- [26] E. Collini, C. Y. Wong, K. E. Wilk, P. M. G. Curmi, P. Brumer, and G. D. Scholes, Coherently wired light-harvesting in photosynthetic marine algae at ambient temperature, *Nature* **463**, 644 (2010).
- [27] G. Panitchayangkoon, D. Hayes, K. A. Fransted, J. R. Caram, E. Harel, J. Wen, R. E. Blankenship, and G. S. Engel, Long-lived quantum coherence in photosynthetic complexes at physiological temperature, *Proc. Natl. Acad. Sci. USA* **107**, 12766 (2010).
- [28] E. Harel and G. S. Engel, Quantum coherence spectroscopy reveals complex dynamics in bacterial light-harvesting complex 2 (LH2), *Proc. Natl. Acad. Sci. USA* **109**, 706 (2012).
- [29] A. Ishizaki and G. R. Fleming, Quantum Coherence in Photosynthetic Light Harvesting, *Ann. Rev. Cond. Matt.* **3**, 333 (2012).
- [30] S. Nakajima, On the quantum theory of transport phenomena, *Prog. Theor. Phys.* **20**, 948 (1958).
- [31] R. Zwanzig, Ensemble method in the theory of irreversibility, *J. Chem. Phys.* **33**, 1338 (1960).
- [32] Q. Shi and E. Geva, A new approach to calculating the memory kernel of the generalized quantum master equation for an arbitrary system-bath coupling, *J. Chem. Phys.* **119**, 12063 (2003).
- [33] A. Kelly and T. E. Markland, Efficient and accurate surface hopping for long time nonadiabatic quantum dynamics, *J. Chem. Phys.* **139**, 014104 (2013).

- [34] J. Cerrillo and J. Cao, Non-Markovian Dynamical Maps: Numerical Processing of Open Quantum Trajectories, *Phys. Rev. Lett.* **112**, 110401 (2014).
- [35] A. A. Kananenka, C.-Y. Hsieh, J. Cao, and E. Geva, Accurate Long-Time Mixed Quantum-Classical Liouville Dynamics via the Transfer Tensor Method, *J. Phys. Chem. Lett.* **7**, 4809 (2016).
- [36] M. Buser, J. Cerrillo, G. Schaller, and J. Cao, Initial system-environment correlations via the transfer-tensor method, *Phys. Rev. A* **96**, 062122 (2017).
- [37] A. Gelzinis, E. Rybakovas, and L. Valkunas, Applicability of transfer tensor method for open quantum system dynamics, *J. Chem. Phys.* **147**, 234108 (2017).
- [38] Y. LeCun, Y. Bengio, and G. Hinton, Deep learning, *Nature* **521**, 436 (2015).
- [39] P. Dollár, V. Rabaud, G. Cottrell, and S. Belongie, Behavior recognition via sparse spatio-temporal features, in *2005 IEEE International Workshop on Visual Surveillance and Performance Evaluation of Tracking and Surveillance* (2005) pp. 65–72.
- [40] D. Weinland, E. Boyer, and R. Ronfard, Action recognition from arbitrary views using 3d exemplars, in *2007 IEEE 11th International Conference on Computer Vision* (2007) pp. 1–7.
- [41] L. Gorelick, M. Blank, E. Shechtman, M. Irani, and R. Basri, Actions as space-time shapes, *Transactions on Pattern Analysis and Machine Intelligence* **29**, 2247 (2007).
- [42] H.-J. Kim, J. S. Lee, and H.-S. Yang, Human action recognition using a modified convolutional neural network, in *Advances in Neural Networks – ISNN 2007*, edited by D. Liu, S. Fei, Z. Hou, H. Zhang, and C. Sun (Springer, Berlin, Heidelberg, Germany, 2007) pp. 715–723.
- [43] A. Klaeser, M. Marszalek, and C. Schmid, A spatio-temporal descriptor based on 3d-gradients, in *Proceedings of the British Machine Vision Conference* (BMVA Press, 2008) pp. 99.1–99.10.
- [44] H. Wang, M. M. Ullah, A. Klaser, I. Laptev, and C. Schmid, Evaluation of local spatio-temporal features for action recognition, in *Proceedings of the British Machine Vision Conference* (BMVA Press, 2009) pp. 124.1–124.11.
- [45] K. Jia and D.-Y. Yeung, Human action recognition using local spatio-temporal discriminant embedding, in *2008 IEEE Conference on Computer Vision and Pattern Recognition* (2008) pp. 1–8.
- [46] J. Liu, S. Ali, and M. Shah, Recognizing human actions using multiple features, in *2008 IEEE Conference on Computer Vision and Pattern Recognition* (2008) pp. 1–8.
- [47] I. Laptev, M. Marszalek, C. Schmid, and B. Rozenfeld, Learning realistic human actions from movies, in *2008 IEEE Conference on Computer Vision and Pattern Recognition* (2008) pp. 1–8.
- [48] J. Liu, J. Luo, and M. Shah, Recognizing realistic actions from videos “in the wild”, in *2009 IEEE Conference on Computer Vision and Pattern Recognition* (2009) pp. 1996–2003.
- [49] G. W. Taylor, R. Fergus, Y. LeCun, and C. Bregler, Convolutional learning of spatio-temporal features, in *Computer Vision – ECCV 2010*, edited by K. Daniilidis, P. Maragos, and N. Paragios (Springer, Berlin, Heidelberg, Germany, 2010) pp. 140–153.
- [50] M. Baccouche, F. Mamalet, C. Wolf, C. Garcia, and A. Baskurt, Action classification in soccer videos with long short-term memory recurrent neural networks, in *Artificial Neural Networks – ICANN 2010*, edited by K. Diamantaras, W. Duch, and L. S. Iliadis (Springer, Berlin, Heidelberg, Germany, 2010) pp. 154–159.
- [51] J. C. Niebles, C.-W. Chen, and L. Fei-Fei, Modeling temporal structure of decomposable motion segments for activity classification, in *Computer Vision – ECCV 2010*, edited by K. Daniilidis, P. Maragos, and N. Paragios (Springer, Berlin, Heidelberg, Germany, 2010) pp. 392–405.
- [52] M. Baccouche, F. Mamalet, C. Wolf, C. Garcia, and A. Baskurt, Sequential deep learning for human action recognition, in *Human Behavior Understanding*, edited by A. A. Salah and B. Lepri (Springer Berlin Heidelberg, Berlin, Heidelberg, 2011) pp. 29–39.
- [53] S. Ji, W. Xu, M. Yang, and K. Yu, 3d convolutional neural networks for human action recognition, *IEEE Transactions on Pattern Analysis and Machine Intelligence* **35**, 221 (2013).
- [54] K. Simonyan and A. Zisserman, Two-stream convolutional networks for action recognition in videos, arXiv:1406.2199 (2014), <https://arxiv.org/abs/1406.2199>.
- [55] D. Tran, L. Bourdev, R. Fergus, L. Torresani, and M. Paluri, Learning spatiotemporal features with 3d convolutional networks, arXiv:1412.0767 (2014), <https://arxiv.org/abs/1412.0767>.
- [56] A. Karpathy, G. Toderici, S. Shetty, T. Leung, R. Sukthankar, and L. Fei-Fei, Large-scale video classification with convolutional neural networks, in *CVPR* (2014).
- [57] L. Sun, K. Jia, D.-Y. Yeung, and B. E. Shi, Human action recognition using factorized spatio-temporal convolutional networks, arXiv:1510.00562 (2015), <https://arxiv.org/abs/1510.00562>.
- [58] J. Yue-Hei Ng, M. Hausknecht, S. Vijayanarasimhan, O. Vinyals, R. Monga, and G. Toderici, Beyond short snippets: Deep networks for video classification, arXiv:1503.08909 (2015), <https://arxiv.org/abs/1503.08909>.
- [59] L. Courtney and R. Sreenivas, Comparison of Spatiotemporal Networks for Learning Video Related Tasks, arXiv:2009.07338 (2020), <https://arxiv.org/abs/2009.07338>.
- [60] S. Hochreiter and J. Schmidhuber, Long short-term memory, *Neural Computation* **9**, 1735 (1997).
- [61] Y. Kim, Convolutional neural networks for sentence classification, arXiv:1408.5882 (2014), <https://arxiv.org/abs/arXiv:1408.5882>.
- [62] X. Shi, Z. Chen, H. Wang, D.-Y. Yeung, W.-k. Wong, and W.-c. Woo, Convolutional lstm network: A machine learning approach for precipitation nowcasting, arXiv:1506.04214 (2015), <https://arxiv.org/abs/1506.04214>.
- [63] S. Chen, S. Zhang, H. Geng, Y. Chen, C. Zhang, and J. Min, Strong Spatiotemporal Radar Echo Nowcasting Combining 3DCNN and Bi-Directional Convolutional LSTM, *Atmosphere* **11**, 569 (2020).
- [64] F. A. Gers, N. N. Schraudolph, and J. Schmidhuber, Learning precise timing with LSTM recurrent networks, *J. Mach. Learn. Res.* **3**, 115–143 (2003).
- [65] Y. Lecun, L. Bottou, Y. Bengio, and P. Haffner, Gradient-based learning applied to document recogni-

- tion, *Proceedings of the IEEE* **86**, 2278 (1998).
- [66] Y. LeCun, K. Kavukcuoglu, and C. Farabet, Convolutional networks and applications in vision, in *Proceedings of 2010 IEEE International Symposium on Circuits and Systems* (2010) pp. 253–256.
- [67] G. Carleo, I. Cirac, K. Cranmer, L. Daudet, M. Schuld, N. Tishby, L. Vogt-Maranto, and L. Zdeborová, Machine learning and the physical sciences, *Rev. Mod. Phys.* **91**, 045002 (2019).
- [68] M. Schuld, I. Sinayskiy, and F. Petruccione, Neural Networks Take on Open Quantum Systems, *Physics* **12**, 74 (2019).
- [69] F. Vicentini, A. Biella, N. Regnault, and C. Ciuti, Variational Neural-Network Ansatz for Steady States in Open Quantum Systems, *Phys. Rev. Lett.* **122**, 250503 (2019).
- [70] A. Nagy and V. Savona, Variational Quantum Monte Carlo Method with a Neural-Network Ansatz for Open Quantum Systems, *Phys. Rev. Lett.* **122**, 250501 (2019).
- [71] M. J. Hartmann and G. Carleo, Neural-Network Approach to Dissipative Quantum Many-Body Dynamics, *Phys. Rev. Lett.* **122**, 250502 (2019).
- [72] N. Yoshioka and R. Hamazaki, Constructing neural stationary states for open quantum many-body systems, *Phys. Rev. B* **99**, 214306 (2019).
- [73] S. Bandyopadhyay, Z. Huang, K. Sun, and Y. Zhao, Applications of neural networks to the simulation of dynamics of open quantum systems, *Chem. Phys.* **515**, 272 (2018).
- [74] B. Yang, B. He, J. Wan, S. Kubal, and Y. Zhao, Applications of neural networks to dynamics simulation of Landau–Zener transitions, *Chem. Phys.* **528**, 110509 (2020).
- [75] L. Bianchi, E. Grant, A. Rocchetto, and S. Severini, Modelling non-markovian quantum processes with recurrent neural networks, *New J. Phys.* **20**, 123030 (2018).
- [76] F. Fassioli, A. Olaya-Castro, S. Scheuring, J. N. Sturgis, and N. F. Johnson, Energy Transfer in Light-Adapted Photosynthetic Membranes: From Active to Saturated Photosynthesis, *Biophys. J.* **97**, 2464 (2009).
- [77] H. van Amerongen, L. Valkunas, and R. van Grondelle, *Photosynthetic Excitons* (World Scientific, Singapore, 2000).
- [78] A. Ishizaki and G. R. Fleming, On the adequacy of the redfield equation and related approaches to the study of quantum dynamics in electronic energy transfer, *J. Chem. Phys.* **130**, 234110 (2009).
- [79] P. Rebentrost and A. Aspuru-Guzik, Communication: Exciton–phonon information flow in the energy transfer process of photosynthetic complexes, *J. Chem. Phys.* **134**, 101103 (2011).
- [80] T. Brixner, J. Stenger, H. M. Vaswani, M. Cho, R. E. Blankenship, and G. R. Fleming, Two-dimensional spectroscopy of electronic couplings in photosynthesis, *Nature* **434**, 625 (2005).
- [81] M. Cho, H. M. Vaswani, T. Brixner, J. Stenger, and G. R. Fleming, Exciton Analysis in 2D Electronic Spectroscopy, *J. Phys. Chem. B* **109**, 10542 (2005).
- [82] J. Strümpfer and K. Schulten, Open Quantum Dynamics Calculations with the Hierarchy Equations of Motion on Parallel Computers, *J. Chem. Theory Comput.* **8**, 2808 (2012).
- [83] D. Kingma and J. Ba, Adam: A method for stochastic optimization, arXiv:1412.6980v8 (2014).
- [84] F. Chollet, “keras”, <https://github.com/keras-team/keras> (2015).
- [85] M. Abadi, A. Agarwal, P. Barham, E. Brevdo, Z. Chen, C. Citro, G. S. Corrado, A. Davis, J. Dean, M. Devin, S. Ghemawat, I. Goodfellow, A. Harp, G. Irving, M. Isard, Y. Jia, R. Jozefowicz, L. Kaiser, M. Kudlur, J. Levenberg, D. Mané, R. Monga, S. Moore, D. Murray, C. Olah, M. Schuster, J. Shlens, B. Steiner, I. Sutskever, K. Talwar, P. Tucker, V. Vanhoucke, V. Vasudevan, F. Viégas, O. Vinyals, P. Warden, M. Wattenberg, M. Wicke, Y. Yu, and X. Zheng, *TensorFlow: Large-scale machine learning on heterogeneous systems* (2015).
- [86] James Bergstra, Dan Yamins, and David D. Cox, Hyperopt: A Python Library for Optimizing the Hyperparameters of Machine Learning Algorithms, in *Proceedings of the 12th Python in Science Conference*, edited by Stéfan van der Walt, Jarrod Millman, and Katy Huff (2013) pp. 13 – 19.
- [87] A. L. Maas, A. Y. Hannun, and A. Y. Ng, Rectifier nonlinearities improve neural network acoustic models, *Proc. ICML* **30**, 3 (2013).
- [88] J. Bergstra and Y. Bengio, Random search for hyperparameter optimization, *J. Mach. Learn. Res.* **13**, 281 (2012).